ESPRI DAWG Memo
Constraints on Astrometric Bias: Comparison of the Simultaneous PRIMA and NACO Measurements of p Eridani During Comm.#17

Neil Zimmerman
Max-Planck-Institut für Astronomie

March 8, 2012

1 Summary

On 2011 Nov 21, the PRIMA commissioning team acquired dual-feed astrometric data on the binary star p Eridani (components HD 10360 and HD 10361; K mag 3.5 and 5.1 respectively; separation $\sim$ 11.5"). In addition to the PRIMA observations, ESO staff allowed us to briefly obtain simultaneous direct adaptive optics images of our target with the NACO system on UT4, in order to provide a diagnostic reference point. After reducing the imaging data, I find the precision of the NACO measurement is limited by errors in the plate calibration, resulting in a 1σ uncertainty of $\pm$13 mas in the R.A. and Dec separation components. The disparity of the NACO separation vector with the corresponding PRIMA measurement is less than 6 mas along each axis. Therefore, the astrometry from the two instruments agree to within the limits of the NACO precision. The most extreme point on the NACO error ellipse (opposite the PRIMA measurement) would imply an astrometric bias of 21 mas, translating to an upper limit on the differential optical path difference (dOPD) bias of 7.4 μm. Here I describe the procedures used to reduce the NACO images, calibrate the plate, and extract the relative astrometry. I also explain the relevant details of the dOPD model used to extract and compare the PRIMA measurement.

2 Observations

Our target and calibration observations are summarized in Table 1. PRIMA's dual fringe-tracking series on p Eri spanned UT 4:16–6:56, comprising 4 "normal" and 3 "swapped" sequences (Figure 2). Beginning at UT 4:49, ESO staff recorded 10 $\times$ 200 0.1091 sec NACO S27 camera exposures of p Eri in the 2.17 μm Brγ filter, accumulating 218 sec in total on the source. To facilitate the rapid "Double_RdRstRd" (read, reset, read) cube readout mode, the detector array was windowed to 512$\times$514 pixels, still comfortably fitting both components of the binary star (Figure 1a)[2]. The typical Strehl ratio of the brighter component of p Eri (HD 10360), as measured by one of the NACO pipeline tasks, was typically 25%. Following the p Eri image acquisition, 10 $\times$ 30 sec exposures of a region of the Trapezium cluster, centered near θ^1 Ori H, were taken to serve as a plate calibration field. Corresponding lamp flats and dark images were acquired on the same night.

Target	Instrument	UT Date (2011 Nov 21)	Airmass	Filter	Exp. Time
p Eri	PRIMA	04:16–06:56	1.26–1.88	K band	951 s (dual fringe-tracking)
p Eri	NACO	04:49–04:57	1.33–1.35	2.17 μm Brγ	$10 \times 200 \times 0.1091$ s
θ^1 Ori H	NACO	05:14–05:27	1.08–1.10	2.17 μm Brγ	10×30.0 s
Dark	NACO	09:33–09:40			3×30.0 s
Dark	NACO	09:43–09:44			3×0.1091 s
Lamp Flat	NACO	09:50–09:54		2.17 μm Brγ	3×4.0 s

Table 1: Summary of PRIMA and NACO observations of p Eri, including calibration frames.

3 Image Processing

I reduced the NACO images with a Python/Pyraf script. First I combined the dark and lamp flat exposure sets via the `dark` and `lampflat` tasks from the `conicap` module of the ESO Eclipse library. Since the lamp flat uses the full detector array, to form a master flat for the 512×514 window used for the p Eri exposures, I extracted the corresponding region to a separate array.

After dark-subtracting and flat-fielding the p Eri and θ^1 Ori H images, the next part of my script selected and replaced bad pixels. Beforehand, I had examined the pixel histogram of each master dark and flat (one for each target) in IRAF `imhist`, to decide on minimum and maximum thresholds for rejecting anomalous pixels. Based on these thresholds, the script formed lists of the bad pixels to replace in each dark-subtracted, flat-fielded target image. Looping through the list, bad pixels were replaced by the median of neighboring, well-behaved pixels. A second iteration was used to replace pixels bordered by too many bad pixels to rely on immediately adjacent neighbors.

The dark subtraction did not remove some large-scale bias structure in the p Eri images. The residual background of these dark-subtracted images had upturned edges at the top and bottom. These artificial ramps, with heights on the order of 10 ADU, posed a problem for the binary target astrometry, since both stars were within the affected regions. To prevent these features from biasing the PSF fits in a later step, for each 0.1091 sec exposure I averaged the 50 leftmost and 50 rightmost data columns to form a mean vertical background profile. To this profile I fitted a one-dimensional smoothing spline, making use of the `scipy.interpolate.UnivariateSpline` class. Since the shape of the residual bias artifact was constant for all detector columns of a given image—to within the read noise scatter, at least—the column-wise subtraction of the smoothed spline accurately flattened the background of each p Eri exposure. Notably, the longer exposure θ^1 Ori H images did not suffer from residual bias structure, so for this data set no such cleaning steps were necessary.

The telescope pointing was fixed throughout each 200-exposure cube of p Eri. Nonetheless, minute tip-tilt errors caused the star images to randomly shift between the 0.1091 sec exposures at the sub-pixel level. Therefore, before co-adding the cleaned p Eri exposures within each cube, I used the pyraf/IRAF `imalign` task to align the exposures. This routine uses interpolation and cross-correlation to determine sub-pixel alignment based on a specified set of reference PSFs. I also tried using the ESO `jitter` program to carry out the shift-and-add, but with unfavorable results: the sky background subtraction component of `jitter` (which could not be disabled from the `gasgano` interface) added spurious negative features around the stars, and in addition the final co-added PSF was not quite as sharp as the `imalign/imcombine` result. In the final co-addition of each p Eri cube, I rejected none of the exposures, given the relatively consistent quality of the PSF upon inspection. One of the ten reduced p Eri images is shown in Figure 1a.

To align the cleaned θ^1 Ori H images, I again used `imalign`. I set the `imalign` parameters so that only the portion of the array common to all exposures was retained, resulting in a final

reduced image with a size of 1022×876 pixels, shown in Figure 1b. The more severe cropping in the vertical direction results from the fact that during the observations, the dithering pattern of the telescope included only up/down (Declination) shifts between exposures. Two kinds of instrumental artifacts survive in the reduced θ^1 Ori H image: a prominent dust diffraction ring (not accounted for in the lamp flat) appears 2" west (right) of TCC 039, and detector persistence between dither pointings caused faint "ghost" PSFs to appear ∼ 1" north of (above) each bright star. Fortunately, these artifacts are all situated far enough from the star PSFs that they could have no effect on the astrometry.

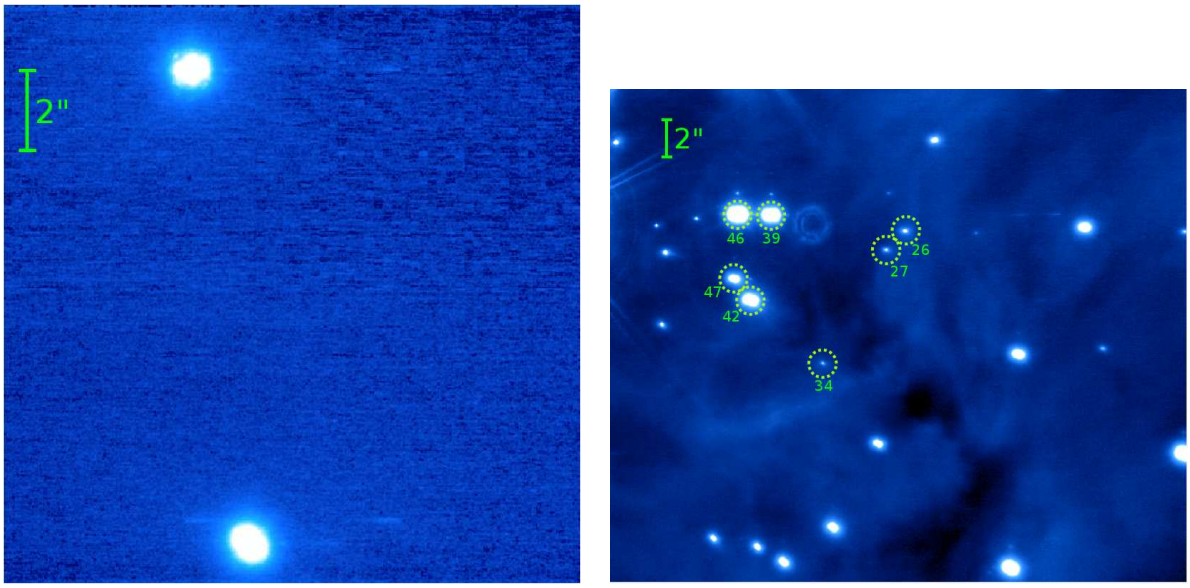

(a) p Eri (b) θ^1 Ori H

Figure 1: Left (a): one of the ten reduced NACO images of p Eri, formed by shifting and adding the 200 exposures of 0.1091 sec integration time within a single cube/pointing. Right (b): The final NACO Trapezium image used for plate calibration, comprised of 10 shifted and added exposures, each of duration 30 sec. The shift-and-add algorithm retained only the image section common to all exposures, hence the final Trapezium image does not span the full 28"×28" NACO field of view. The Trapezium stars with calibrated astrometry available from 2011 Oct 16 LBT data are circled and labeled according to their TCC number (after McCaughrean & Stauffer 1994). Both images are displayed with a square-root stretch to reveal the background noise structure.

4 PSF Position Measurements

To fit the star PSFs in my reduced images and therefore determine their relative positions, I followed the NACO image treatment of Eva Meyer, described in Chap 4 of her PhD dissertation on AO astrometry [8]. She found that the `MPFIT2DPEAK` function, part of Craig Markwardt's MPFIT library for IDL [6], gives reliable fits to NACO PSFs. The user can configure `MPFIT2DPEAK` to model the given PSF with a Moffat function defined by two orthogonal characteristic widths, a rotation, and a fixed power law fall-off index. The free parameters in this function allow me to match the "radial breathing"—the elongation of the PSF away from the guide star, which is prominent in all of the images.

To apply `MPFIT2DPEAK`, the user must decide the dimensions of the box to cut out around

the given star and feed into the model. In the case of the reduced p Eri images, where the SNRs of the two binary components are $\sim$ 5000 and 10000, we followed Meyer's method of using a 31×31 pixel box that extends well into the wings of the PSF (FWHM $\sim$ 2.5 pixels). In the θ^1 Ori H image, on the other hand, nebulosity associated with the star forming region provides significant contamination that could bias the PSF fits, particularly for the fainter stars (see Figure 1b). Therefore, I truncated the fitting box to include only the area where the star dominates over any features in the surrounding emission, from visual inspection. My smallest fitting box had dimensions 15×15 pixels, used only for the faintest star I measured, TCC 034.

To extract the uncalibrated separation vector from the p Eri data, I fitted the pair of PSFs in each of the 10 reduced images and average the position difference vectors. To estimate the precision, I took the standard deviation of each component across the 10 images. The resulting horizontal and vertical pixel offsets measured from HD 10360 (northern component) to HD 10361 (southern component) are 51.369 ± 0.036 and -418.499 ± 0.050. At the nominal NACO pixel scale, 27.15 mas/pixel, these standard deviation values correspond to 1.0 mas and 1.4 mas, respectively.

For the angular scales and zenith angles we encounter in our target and calibration images, differential refraction is not negligible. At the median airmass of our p Eri NACO images, for example, secz = 1.34 (zenith angle 41.7°), differential refraction causes an apparent contraction of the celestial sphere by 0.036% in the zenith direction. The necessary compensation amounts to about 2.7 mas, given the 7.5" separation of the binary components projected along the altitude direction.

Following the approach of Meyer again, I used the differential refraction relations of Gubler & Tytler [3] to correct our relative star positions for this distortion. The additional chromatic component of differential refraction is expected to be a factor of $\sim$ 20 smaller for a moderate range of star temperatures (3000 K) and angular separations (15"), so I did not attempt to take this into account [8]. Besides the wavelength and zenith angles, the Gubler & Tytler relations require knowledge of the ground layer temperature and pressure to adjust the correction for local atmospheric conditions. I used the ambient temperature and pressure values recorded in the FITS headers of our NACO images. These values remained relatively stable throughout our NACO observations, in all cases decreasing the differential refraction correction by about 9% as compared to the compensation predicted for nominal environmental conditions.

5 Plate Calibration

Rainer Köhler made large contributions to this stage of the analysis, having unique knowledge of, and access to, Trapezium cluster astrometry, along with software tools to compute and interpret the plate transformation. In our plate calibration approach, we used a comparison between our own differential refraction-corrected PSF positions in the θ^1 Ori H field and our best knowledge of the corresponding stars' true celestial coordinates in order to derive a plate scale and orientation. We used the `ASTROM` program by Patrick Wallace to compute the plate transformation[12].

The Trapezium cluster has been used by previous NACO observers as a plate calibration field, since it is relatively bright and dense. For example, Chauvin et al. (2012) used a region of the Trapezium to calibrate the relative astrometry of the β Pic planet, and eventually derive an orbit fit [1]. In retrospect however, this field, or at least the region we observed, is not the best suited to calibrate our data. The main problem is the lack of up-to-date, published astrometry of star cluster members, particularly the fainter ones (all stars in our field have $V > 13$, out of reach of existing proper motion surveys). In their calibration, Chauvin et al. used the coordinates published by McCaughrean & Stauffer (1994), measured in 1993 with the

MAGIC/CHARM camera at Calar Alto Observatory with tip-tilt correction [7].

The velocity dispersion of the Orion cluster, measured through proper motion analysis of brighter members, is $\sim$ 2 km/s, which translates to $\sim$ 1 mas/yr for the distance of the Trapezium [5, 11]. Therefore, the intrinsic motion of these stars poses a problem for achieving milliarcsec-precision plate calibration with reference coordinates older than 10 years, particularly since we are trying to calibrate a relatively large (11.4") separation vector. Fortunately, Rainer Köhler had privileged access to still unpublished Trapezium astrometry acquired with the LBT on 16 October 2011, close to one month before our p Eri observations. The caveat is that only seven of the stars with LBT position measurements are in our field of view. These stars are marked in Figure 1b; here we list their TCC indices, as designated by McCaughrean & Stauffer (1994): 026, 027, 034, 039 (θ^1 Ori H 1), 046 (θ^1 Ori H), and 047. Using our refraction-corrected positions and the recent LBT astrometry as input, we applied `ASTROM` to arrive at the plate scale and orientation given in Table 2. The 1σ error bars are computed in a script by Köhler which determines the residual scatter for the given plate solution. For a pair of stars with separation of p Eri, 11.4", the uncertainty in the plate calibration scales to 13 mas in the radial direction and 12 mas in the tangential direction. Applying our plate transformation to the p Eri offsets measured in the NACO images, and then correcting for differential refraction in the same way as described in the previous section, gives the separation vector described in Table 3.

Plate Scale	Plate Orientation (counter-clockwise, from image vertical to true north)
27.130 $\pm$ 0.032 mas/pix	-0.788 $\pm$ 0.059°

Table 2: NACO plate solution derived from applying `ASTROM` to the position measurements of the reference stars marked in Figure 1b.

6 Comparison with the PRIMA Solution

To extract the astrometry from the 2011 Nov 21 PRIMA data, Johannes Sahlmann and I fitted a separation vector to the reduced metrology in the intermediate data file. Most of the data processing steps necessary to produce this intermediate file from the raw PRIMA data are described in an internal ESO VLTI report distributed by Sahlmann in 2011 [9]. From the reduced sequence of differential optical path difference (dOPD) measurements, we apply a non-linear least-squares fit to determine the most probable target configuration based on the description by Damien Ségransan [10]. In his report, Ségransan derives the equations relating the dOPD metrology to the celestial coordinates of the pair of dual-feed target stars, the local sidereal time, the observatory latitude, and the interferometer baseline. We note that the baseline we assume for this data set is not the vector specified in the data file header, but rather a revised one calculated by Sahlmann through a method he will document in his PhD dissertation. Thus, we changed the baseline vector (in meters east, north, and up) in our dOPD model from $(49.8678, -76.3731, -0.0147)$ to $(49.87766, -76.387910, -0.017539)$. In our fit, we only included metrology acquired in dual fringe-tracking mode, which showed less noise than the scanning mode data. For consistency with the NACO astrometry, inside the dOPD model we also corrected each reduced metrology point for differential refraction, based on the same principles we described earlier.

The PRIMA dOPD data and the best-fit model are plotted in Figure 2. The root-mean-square value of the dOPD fit residual is 0.60 microns. The PRIMA astrometry vector associated

with this best-fit model, along with the corresponding NACO measurement and their difference, is given in Table 3. In Figure 3, I plot both relative astrometry results along with the NACO error ellipse, whose dimensions are set by the uncertainty in the plate scale and orientation. From the plot, it is clear that the PRIMA separation vector agrees within the 1σ error ellipse of the NACO point.

Our dOPD model allows us to translate a given hypothesis for the "true" astrometric configuration of the binary star into a corresponding estimate of the systematic error in the PRIMA metrology. For a given set of fixed primary–secondary star offsets, I evaluate the dOPD model at the same times as our reduced PRIMA metrology samples, and subtract the results from our measured dOPD to find the residuals. The mean of this residual array gives a measure of the bias that would have to be present in the dOPD to make up the disparity. There is one extra step before this, because to evaluate the dOPD for each hypothesis, in addition to the star coordinates, we need a metrology zero point constant to reconcile the optical path difference between the normal and swapped observation modes. Normally this zero point is fit as a free parameter at the same time as the binary separation vector to the data. I optimize the zero point again for each proposed offset vector, so as to minimize the least-square residuals model while leaving the star positions fixed. (If we do not re-optimize the zero-point, we tend to slightly overestimate the bias.) In this way, I determined the bias for two test cases: the NACO measurement, and the point on the NACO error ellipse directly opposite the PRIMA point. If we assume the NACO measurement is the true separation vector—8.1 mas away from the PRIMA point, as given in Table 3 and Figure 3—then the dOPD bias is 2.9 microns. At the more extreme case, the point on the error ellipse opposite the PRIMA measurement, 20.9 mas from the PRIMA point, the dOPD bias would be 7.4 microns.

A discussion of systematic error sources in the PRIMA data is beyond the scope of this report. However, it is interesting to note that the scale of the residuals of the astrometric solution plotted in the lower half of Figure 2—in particular, the arcing trend between fringe-locked sequences—is of the same order as the 3 micron NACO disparity.

In the interest of improving the plate calibration, and therefore placing stronger constraints on possible systematic errors in the PRIMA data, I sought the advice of Gaël Chauvin (MPIA/LAOG). In his opinion, the uncertainty we have in our separation vector, $\sim \pm 0.1\%$ in each component, is as tight as can be expected with one reference star field. To measure position-dependent image distortions and add higher order terms to our plate solution, for example, would have required more planning and reference stars. His research group has not yet had a need to take this step, since the Beta Pic B astrometry is limited by other effects, but he did suggest the names of a few experts to contact (e.g., Stefan Gillessen of MPE), in case the DAWG chooses to pursue this further. In particular, it is possible the galactic center group at MPE would be willing to share a proprietary map of optical distortions in the NACO S27 camera (see Fritz et al. 2010 for a description of their approach to astrometric calibration [4]).

Description	$\Delta\alpha \cos\delta$ (mas)	$\Delta\delta$ (mas)	ρ (mas)	θ (deg)
PRIMA	-1557.4	-11329.3	11435.8	187.83
NACO	-1551.9	-11335.1	11440.9	187.80
Difference (PRIMA − NACO)	-5.5	5.9	-5.1	0.03

Table 3: Comparison between the NACO and PRIMA relative astrometry of p Eridani. After the Right Ascension and Declination offsets, we specify the radial separation (ρ) and the position angle (θ, in degrees counter-clockwise of north).

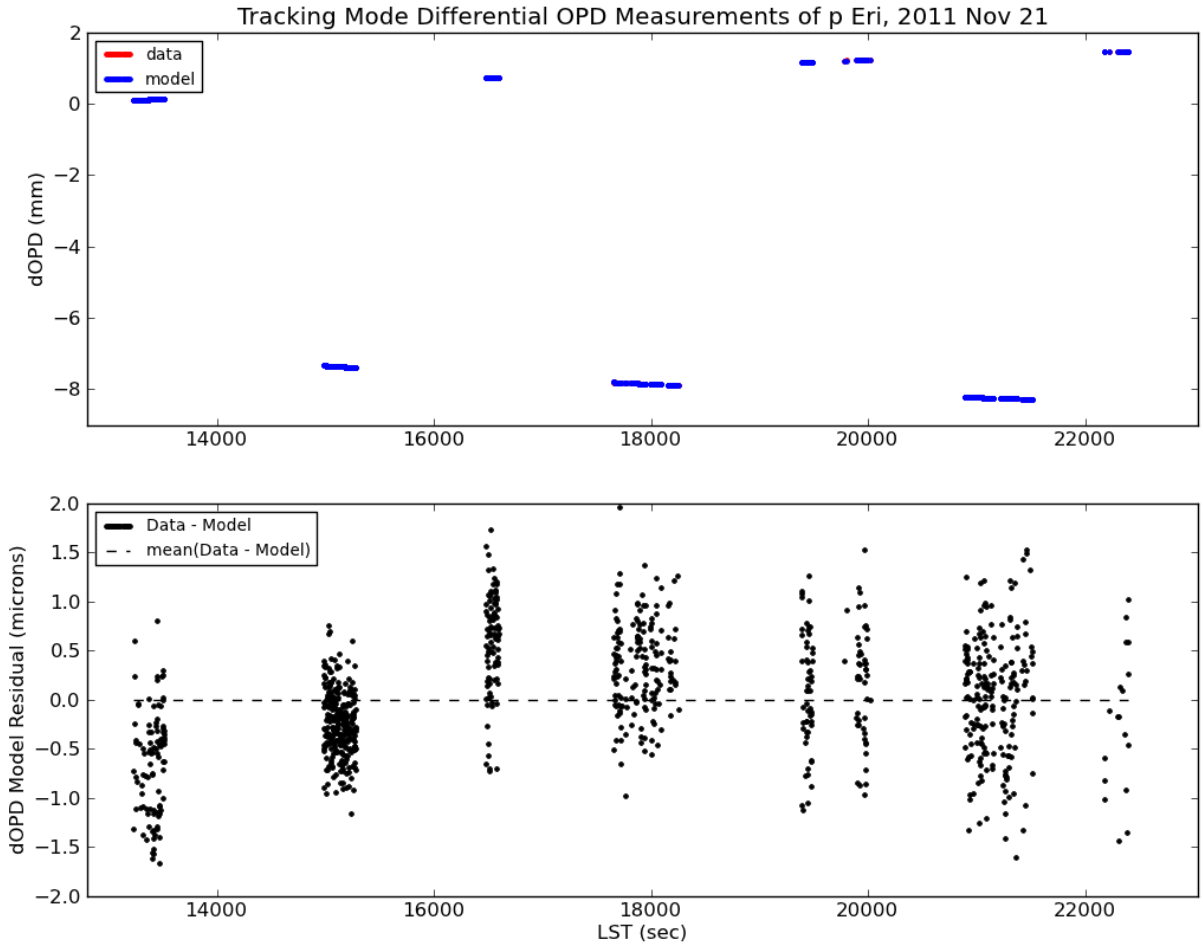

Figure 2: Top: the differential OPD (dOPD) measured from PRIMA data, including only data recorded in dual fringe-tracking mode as opposed to scanning mode. The over-plotted model, the dOPD expected from the best-fit double star configuration given the assumed PRIMA baseline, is indistinguishable from the data on a millimeter scale. Bottom: the residual of the dOPD fit, which has a root-mean-square value of 0.60 μm.

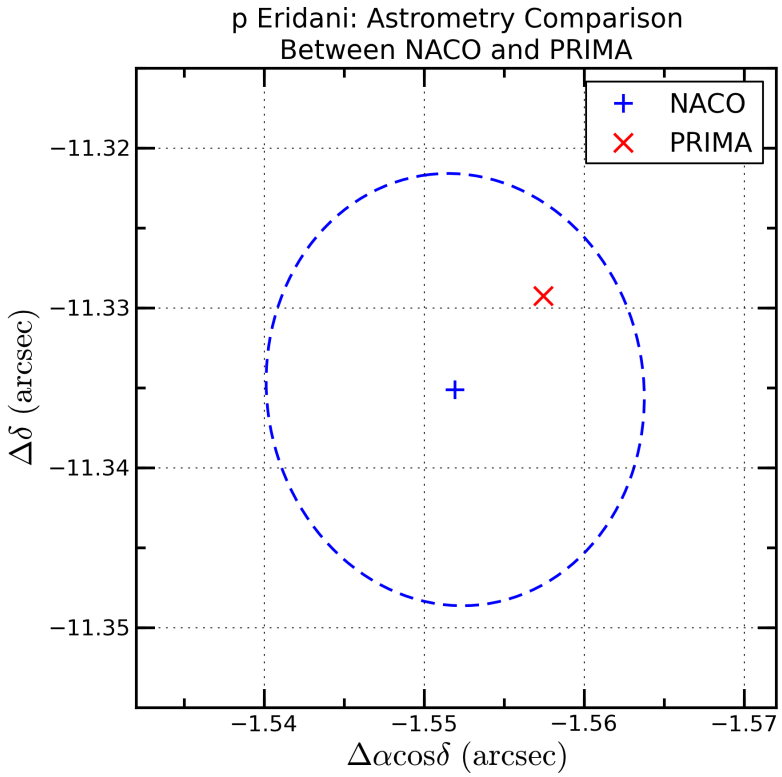

Figure 3: The error ellipse of the p Eridani separation vector measured with NACO, alongside the separation vector from the PRIMA astrometric solution. The statistical uncertainty of the PRIMA result is smaller than the plotting symbol, so it is not shown.

References

[1] Chauvin, G., Lagrange, A.-M., Beust, H., et al. 2012, arXiv:1202.2655

[2] Girard, J. 2012, *Very Large Telescope NACO User Manual*, Issue 90.1.

[3] Gubler, J., & Tytler, D. 1998, *PASP*, 110, 738.

[4] Fritz, T., Gillessen, S., Trippe, S., et al. 2010, *MNRAS*, 401, 1177

[5] Jones, B. F., & Walker, M. F. 1988, *Astronomical Journal*, 95, 1755

[6] Markwardt, C. B. 2009, Astronomical Data Analysis Software and Systems XVIII, 411, 251

[7] McCaughrean, M. J., & Stauffer, J. R. 1994, *Astronomical Journal*, 108, 1382

[8] Meyer, E., 2010. PhD Dissertation: *High Precision Astrometry with Adaptive Optics aided Imaging*, Chap 4, available on arXiv at `http://arxiv.org/abs/1005.5091`.

[9] Sahlmann, J. 2011, *PRIMA astrometry data modelling and analysis of auxiliary data (Comm14)*, VLT-TRE-ESO-15770-5337

[10] Ségransan, D. and Weber, L. 2007, *APES Design Report*, VLT-TRE-AOS-15751-0003

[11] Tian, K. P., van Leeuwen, F., Zhao, J. L., & Su, C. G. 1996, *Astronomy and Astrophysics Supplement*, 118, 503

[12] Wallace, P. T. 1998. *ASTROM: Basic astrometry program v3.6 User's Guide*, published as Starlink User Note 5.17 from the CCLRC Rutherford Appleton Laboratory.